Catal Lett (2007) 118:280–284
DOI 10.1007/s10562-007-9188-4

Tungsten Trioxide Films with Controlled Morphology and Strong Photocatalytic Activity via a Simple Sol–Gel Route

Bin Yang · Piers R. F. Barnes · Yingjie Zhang · Vittorio Luca

Received: 23 August 2006 / Accepted: 1 December 2006 / Published online: 21 August 2007

Abstract Novel nanostructured tungsten trioxide (WO_3) films with strong photocatalytic activity, have been prepared by a simple sol–gel route from aqueous peroxopolytungstic acid (PTA) precursor solutions. We demonstrate that films with different morphologies can be synthesized by simply adjusting the pH of this precursor solution using different mineral acids such as HCl and $HC1O_4$, and that this control of film texture represents a way of optimizing photocurrent yield. The best films produced using these methods generated anodic photocurrents of 3.8 mA/cm^2 for oxidiation of methanol and 2.2 mA/cm^2 for water splitting, under AM1.5 simulated solar illumination.

Keywords Photocatalytic activity · Sol–gel · Tungsten trioxide · Photocurrent · Water splitting

1 Introduction

Tungsten trioxide (WO_3) is an *n*-type semiconductor with a range of potential applications including: gas sensing [1, 2], electrochromic windows and displays [3–6], catalysis [7] and photooxidation of water [8–13]. The ultimate of this study is to prepare efficient, adherent, chemically- and electrochemically-stable WO_3 films with high photocatalytic activity which can be used for water splitting using sun light.

Tungsten trioxide films can be synthesized by several different physical and chemical techniques such as vapor deposition, sputtering, electrodeposition [13–15] and sol–gel processing [4–6, 16]. The sol–gel method in particular has several advantages, namely: low cost, ease with which large surfaces can be coated, control of film thickness, and the ability to prepare a range of mesoporous structures. The preparation and properties of mesoporous WO_3 films using block copolymer as a template have been studied by two research groups [4, 16]. The results showed that these mesoporous films exhibit excellent electrochromic response and optical reversibility, after calcination at 300 °C. However, the mesoporous structure collapses after calcination at 400 °C during the crystallization of WO_3. Unfortunately, in the case of photoelectrochemical splitting of water, high crystallinity is a prerequisite. For instance, Santato et al. [11] showed that a temperature of at least 550 °C is required to achieve a crystallinity giving optimum photoresponse. Consequently there is a need to develop methods for producing WO_3 films having both high crystallinity, and a texture with good intra-particle contacts. In this communication, we report a very simple method for producing nanostructured WO_3 films without using surfactants to template the structure.

The approach described here generates nanostructured WO_3 films from an aqueous precursor solution of peroxopolytungstic acid (PTA) by careful adjustment of pH using different mineral acids. This method results in various self-assembled porous films consisting of inter-connected particles (0.3 μm) formed during the colloidal condensation. It boasts several advantages including: (1) simplicity and low cost; (2) no templating surfactant is required; (3) control of morphology by the adjusting the precursor chemistry; (4)

B. Yang (✉) · Y. Zhang · V. Luca
Australian Nuclear Science and Technology Organisation, PMB 1, Menai, NSW 2234, Australia
e-mail: byz@ansto.gov.au

P. R. F. Barnes
CSIRO Industrial Physics, P.O. Box 218, Lindfield, Sydney, NSW 2070, Australia
e-mail: piers.Barnes@csiro.au

the resulting structures have high thermal stability up to 550 °C; (5) the films show good photocatalytic activity—generating high photocurrents as photoanodes.

2 Experimental

WO_3 films were synthesized by a sol–gel route from an aqueous precursor containing PTA electrolyte. The precursor was prepared in the following manner: (1) dissolving 1.8 g of tungsten powder (Aldrich Chem. Co, 99.9%) in 60 mL of 30% hydrogen peroxide for about 6 h; (2) decomposing the excess hydrogen peroxide by adding a small amount of platinum black (Aldrich Chem. Co); (3) diluting the solution to 0.1 M by adding about 50 mL of 2-propanol to improve the stability. The resulting precursor had a pH of 1.58. The precursor pH was then adjusted to values in the range 0.2–1.58 by adding mineral acids, such as HC1 and $HC1O_4$. This changed the appearance of the subsequent calcined films from transparent to semi-transparent. The thin films were deposited by doctor Blading or drop casting the precursor solution onto conducting indium doped tin oxide (ITO) coated glass at room temperature and then drying at 60 °C. Finally, as-deposited films were calcined in air at 500 °C for 30 min to form a crystalline WO_3 layer. After calcination, the films were strongly adherent to the ITO glass. Thick and homogeneous films were made by repeating deposition-calcination cycles.

In this paper, we report three films synthesised with precursors of pure PTA (referred to as film a, pH 1.58), PTA + HC1 (film b, pH = 0.3) and PTA + $HC1O_4$ (film c, pH = 0.6). The films with different nano-structures formed through the colloidal condensation of the precursor species during the evaporation of solvent at 60 °C. We have observed that the porous structure is preserved up to a calcination temperature of 550 °C.

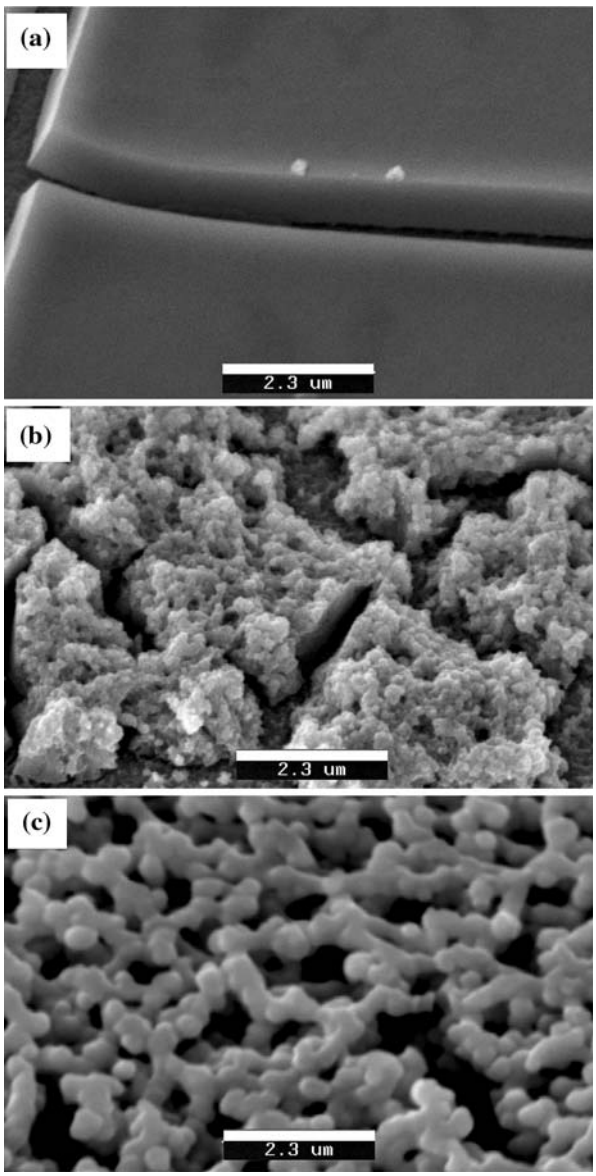

Fig. 1 The SEM images of films **a**, **b** and **c**

3 Results and Discussion

The SEM images of films a, b and c are shown in Fig. 1. Film a is visually transparent, while films b and c are semi-transparent. This visual change is due to changes in the morphology, density and texture. Film a has a very smooth surface, with the presence of a few micro-cracks. Thicknesses exceeding 1.8 μm had a tendency to peel off at elevated temperature. Film b had a very rough surface with a high density of micro-cracks, it consists of particle clusters, about 130 nm in diameter. This film generated the highest photocurrent, possibly due to the good contact between the WO_3 layer and the conducting substrate, and high density of cracks which could allow improved electrolyte transport. Film c has a very interesting porous structure which consists of an open 3D network of interconnected droplet-like particles with diameters in the range of 100–300 nm. This structure also allows electrolyte to enter the 3D network easily, consequently improving electron conductivity at the interface and increasing the effective surface area of the WO_3 layer.

Figure 2 shows the X-ray diffraction patterns of the three films after being calcined at 480 °C for 30 min, and one as-deposited film. For all the films prior to calcination, the WO_3 layer is amorphous at room temperature and is characterized by a very broad hump centred at $2\theta = 25°$. After calcination, several sharp peaks appear in the diffraction patterns, indicating the formation of the monoclinic WO_3 crystalline phase with the lattice parameters: $a = 7.301$, $b = 7.498$, $c = 7.670$, $\alpha = 90°$, $\beta = 90.91$

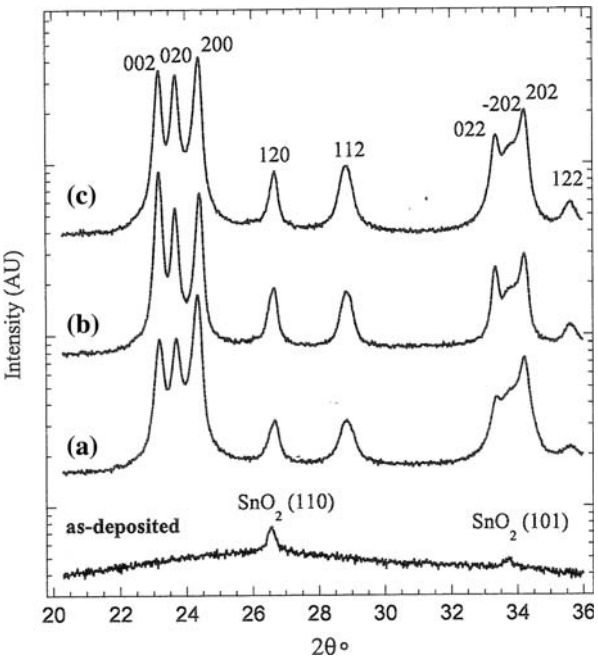

Fig. 2 (Color Online) X-ray diffraction patterns of films **a**, **b** and **c**, after been annealed at 480 °C. Diffraction pattern of as-deposited film is also shown. The two sharp peaks are contributions from the conducting SnO_2 substrate. Ni filtered Cu kα-radiation (λ = 0.154 nm) was used

and $\gamma = 90°$. In addition, the correlation length of the crystalline phase can be evaluated from the Scherrer equation by taking the values of full width at half maximum (FWHM = 0.45°) of the peak (112). This analysis shows that the correlation length is about 18 nm for a, b and c. It is evident the crystallite size is independent of acid used. However, the different mineral acid used strongly influences the assembly of texture in the films. The connectivity of these particle aggregates is also dependent on the mineral acid and determines the porosity at the macro length scale.

Figure 3 shows absorption spectra of the films with the absorption onset at approximately 480 nm. The band gap of all the films is 2.6 eV corresponding to an indirect band gap of purely crystalline WO_3 [17]. These values are determined using a Tauc plot which shows the square root of the Kubelka–Munk unit of absorption (KMU) multiplied by photon energy as a function of photon energy (Fig. 3 inset). The absence of any significant red- or blue-shift suggests that the different morphologies of the films do not influence the band gap. However, a notable difference between the films is that the integral of the absorption spectra for b and c is about 40 and 20% larger than that of film a, respectively. The more effective absorption of light by the semi-transparent material probably results from an increased path length of light in the film due to scattering from the 3D network and particles.

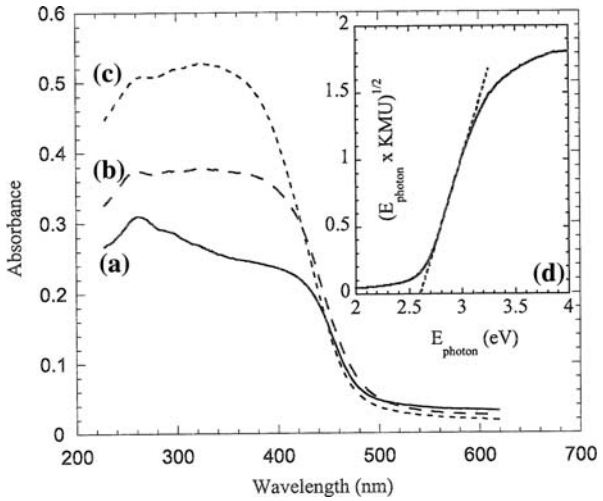

Fig. 3 (Color Online) The absorption spectra of films **a**, **b** and **c**. The band gap of all films is 2.6 eV, determined by the Tauc plot (inset)

The electrochemical response of the three film types, after being annealed at 120 °C for 10 min, was examined by using cyclic voltammetry (CV). The films have the same specific mass of 0.5 mg/cm^2. Figure 4 shows the cyclic voltammograms for hydrogen intercalation–deintercalation for the films in 1 M of sulfuric acid. Clearly, b and c show greater currents for both intercalation and deintercalation than a. This is induced by the nanostructure and the rough surface of films b and c. During the CV, the color of the film changes reversibly from pale yellow to dark blue on reduction, and it reverts to pale yellow during anodization. These effects are due to the reversible changes between WO_3 and the blue-colored tungsten bronze (H_xWO_3) [5].

The photoelectrochemical response of the films was determined by measuring the photocurrent under an illumination of 86 mW/cm^2, (Oriel, 1,000 W ozone-free water filtered Xe lamp measured using a thermopile detector) [18]. Photocurrent is given by the difference between light and dark time-stable current densities where dark current is typically <30 μA/cm^2, charge transferred as photocurrent without the presence of methanol is contributed to participate in the O_2 and H_2 evolution reactions. The photocurrent as a function of layer thickness was measured and the optimum thickness for films b and c found to be 2.3 and 2.8 μm, respectively. Figure 5 shows the photocurrent of the best of each type of film as a function of potential, in 1 M H_2SO_4 where film thicknesses are 1.8 μm (a), 2.3 μm (b) and 2.8 μm (c). Film b generates the largest saturation photocurrent of 2.4 mA/cm^2. The equivalent photocurrent under AM 1.5 solar illumination can be estimated by multiplying by the ratio of integrated photon fluxes with energies greater than the band gap in the photon flux spectra of AM 1.5 and the xenon lamp to give

2.4*0.78*100/86 mA/cm^2 = 2.2 mA/cm^2 [18]. Film c produces a saturation photocurrent about 1.4 mA/cm^2. The photocurrent of film a is lower (about 0.5 mA/cm^2) which is in part due to it being a thinner film and hence absorbing less incident light than the others.

Curves b′ and c′ in Fig. 4, show photocurrents exceeding 4 mA/cm^2 (equivalent to 3.8 mA/cm^2 under AM 1.5) for films b and c, which were obtained after the addition of 0.1 M of methanol as a sacrificial electrolyte to the cell. It is evident that the oxidation of methanol induces a significant (2 to 3-fold) increase in photocurrent and a reduction by about 0.2 V of the current onset potential. This phenomenon can be explained by the photocurrent doubling effect where an additional electron is injected in the conduction band of the electrode during the photodecomposition of methanol [19]. This result is in general agreement with that reported by Santato et al. [11]. However, they observed only a doubling of the photocurrent with the addition of methanol. In our case, for film c, the saturated photocurrent can be about three times higher after addition of methanol to the electrolyte. The uniquely textured film may play an important role in the anomalous increase in photocurrent for oxidation of methanol relative to water, however, the reason for this deviation from photocurrent doubling is not clear. Further study is required to clarify this observation.

4 Conclusions

We have demonstrated that the addition of different mineral acids to peroxopolytungstate solutions can strongly influence the texture of WO_3 films formed and result in an enhanced photoresponse. Based on our experimental results, we conclude the following: (1) Uniform porous, semi-transparent WO_3 films can be fabricated through controlled acidification of peroxopolytungstate solutions used for film deposition. The best semi-transparent film prepared here can produce 3.8 and 2.2 mA/cm^2 photocurrent under simulated AM 1.5 sun light, in 1 M H_2SO_4 with and without 0.1 M methanol respectively; (2) The three films have approximately the same band-gap. However, the semi-transparent films absorb more UV light than the transparent film probably due to light scattering within the film; (3) Films b and c have higher photocatalytic activity which results from their distinct nano-textures rather than bandgap shift or doping effects; (4) Porous films such as those produced here could have potential applications as photocatalytic materials. The easily prepared porous interconnected structure might also offer some advantages in gas sensing and electrochromic applications.

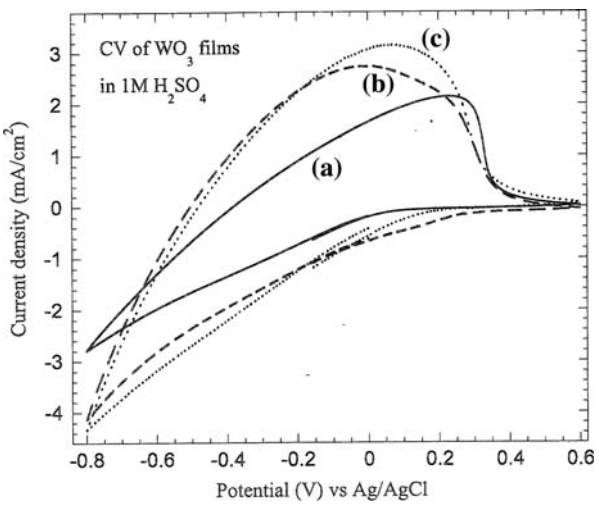

Fig. 4 (Color Online) Cyclic voltammograms (CV) of the WO_3 films, scan rate 3O mV/s, in 1 M of sulfuric acid. Films **b** and **c** have greater currents for both intercalation and deintercalation than a

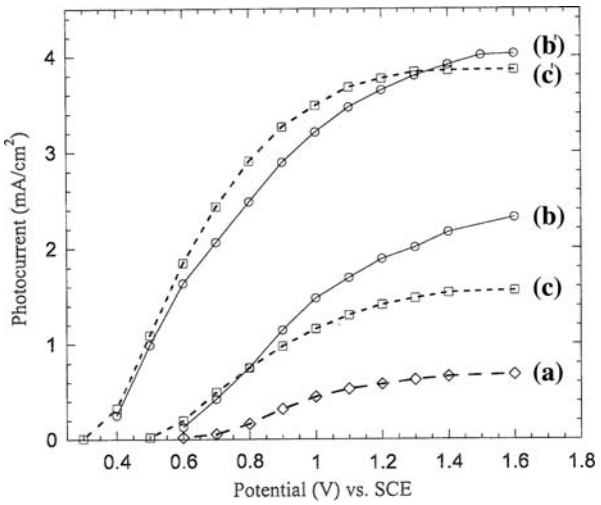

Fig. 5 (Color Online) The photocurrent of the films irradiated by a xenon lamp (86 mW/cm^2). The curves (a), (b) and (c) are the photocurrents of the films **a**, **b** and **c** respectively in a electrolyte of 1 M H_2SO_4. The curves (b′) and (c′) represent photocurrent of films **b** and **c**, was measured by using an electrolyte of 1 M H_2SO_4 with 0.1 M of methanol

References

1. Cantalini C, Lozzi L, Passacantando M, Santucci S (2003) IEEE Sens J 3(2):171
2. Tamaki J, Okochi Y, Konishi S (2006) Electrochemistry 74(2):159
3. Deepa M, Sharma R, Basu A, Agnihotry SA (2005) Electrochim Acta 50:3545
4. Cheng W, Baudrin E, Dunn B, Zink JI (2001) J Mater Chem 11:92
5. Leftheriotis G, Papaefthimiou S, Yianoulis P, Siokou A, Kefalas D (2003) Appl Surf Sci 218:275
6. Munro B, Kramer S, Zapp P, Drug H (1998) J Sol–gel Sci Technol 13:673

7. Habazaki H, Hayashi Y, Konno H (2002) Electrochim Acta 47:4181
8. Wang H, Lindgren T, He J, Hagfeldt A, Lindquist SE (2000) J Phys Chem B 104:5686
9. Miller EL, Marsen B, Cole B, Lum M (2006) Electrochem Solid-State Lett 9(7):G248
10. Erbs W, Desilvestro J, Borgarello E, Gratzel M (1984) J Phys Chem 88:4001
11. (a) Santato C, Ulmann M, Augustynski J (2001) J Phys Chem B 105:936, (b) Santato C, Odziemkowsld M, Ulmann M, Augustynski J (2001) J Am Chem Soc 123:10639
12. Berger S, Tsuchiya H, Ghicov A, Schmuki P (2006) Appl Phys Lett 88:203119
13. (a) Baeck SH, Jaramillo T, Stucky GD, McFarland EW (2002) Nano Lett 2(8):831, (b) Baeck SH, Choi KS, Jaramillo TF, Stucky GD, McFarland EW (2003) Adv Mater 15:1269, (c) Baeck SH, Jaramillo TF, Brandli C, McFarland EW (2002) J Comb Chem 4:563
14. Meulenkamp EA (1997) J Electrochem 144(5):1664
15. Yang B, Li HJ, Blackford M, Luca V (2006) Current Appl Phys 6(3):436
16. Teoh LG, Shieh J, Lai WH, Hon MH (2004) J Mater Res 19(9):2687
17. Butler MA (1997) J Appl Phys 48(5):1914
18. Murphy AB, Barnes PRF, Randeniya LK, Plumb IC, Grey IE, Home MB, Glasscock JA (2006) Int J Hydrogen Energy (in press)
19. Morrison SR, Freund T (1967) J Chem Phys 47(4):1543